

Dual-defect sites regulation on MOF-derived P-Co₃O₄@NC@O_v-NiMnLDH carbon arrays for high-performance supercapacitors

Fangfang Zhu,^a Lin Sun,^a Yu Liu,^a and Weidong Shi^{a,*}

^a School of Chemistry and Chemical Engineering, Jiangsu University, Zhenjiang, 212013, P. R. China.

*E-mail: swd1978@ujs.edu.cn. Tel: +86-511-88791800

Experimental Section

preparation of CNT@ZIF-8 derived C

100 ml methanol solution containing 50 mg CNTs was sonicated for 1 h, then 0.35 g $\text{Zn}(\text{NO}_3)_2 \cdot 6\text{H}_2\text{O}$ was added and stirred for 1 h to form solution A. Solution B is a 50 ml methanol solution that dissolves 1.052 g of 2-methylimidazole. Then add solution B to solution A, stir for 1 h, stand at room temperature for 24 h, centrifugally wash and collect samples, and calcine at 800 °C for 2 h.

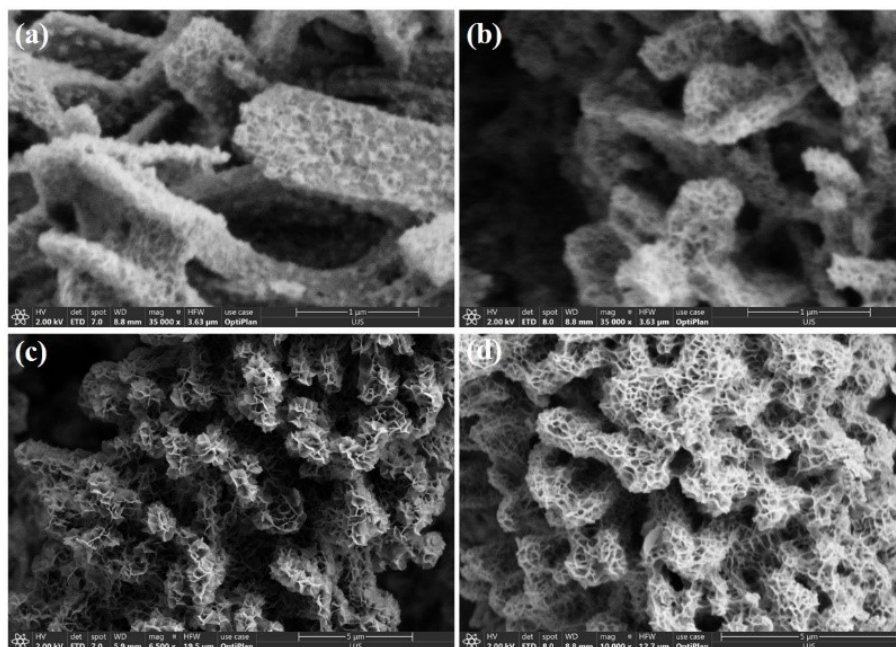


Fig. S1 The SEM image of P-Co₃O₄@NC@NiMnLDH with different reaction time (a) 4 h, (b) 6 h, (c) 8 h, (d) 10 h.

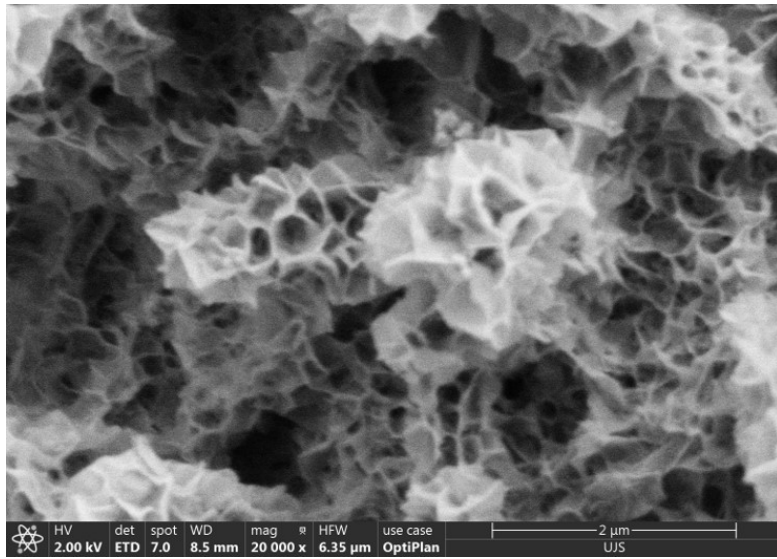


Fig. S2 The SEM image of P-Co₃O₄@NC@NiMnLDH.

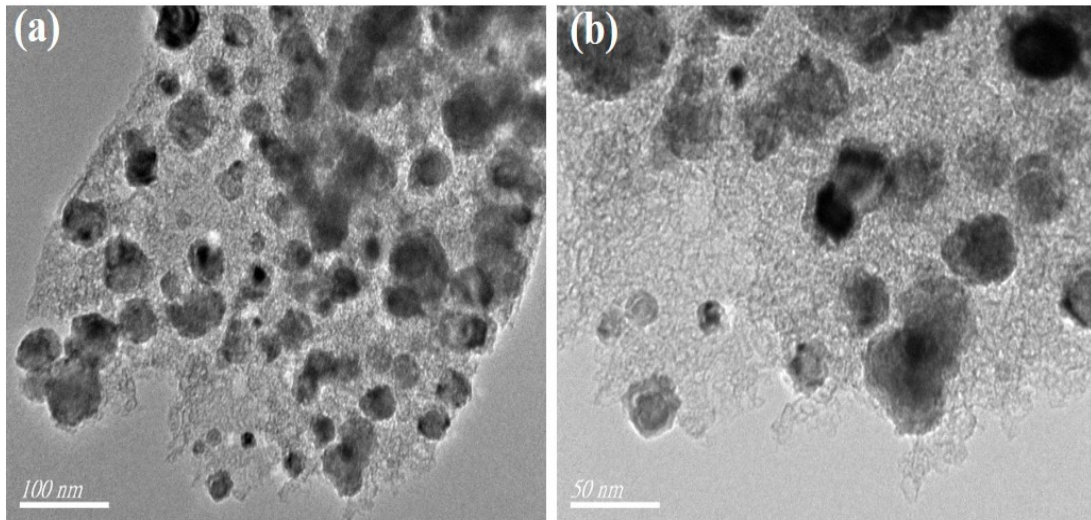


Fig. S3 The TEM image of Co@NC.

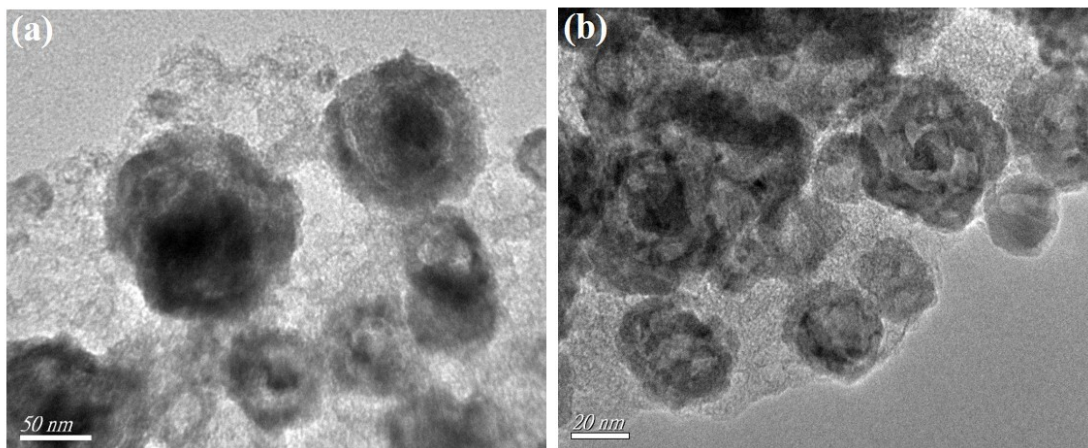


Fig. S4 The TEM image of P-Co₃O₄@NC.

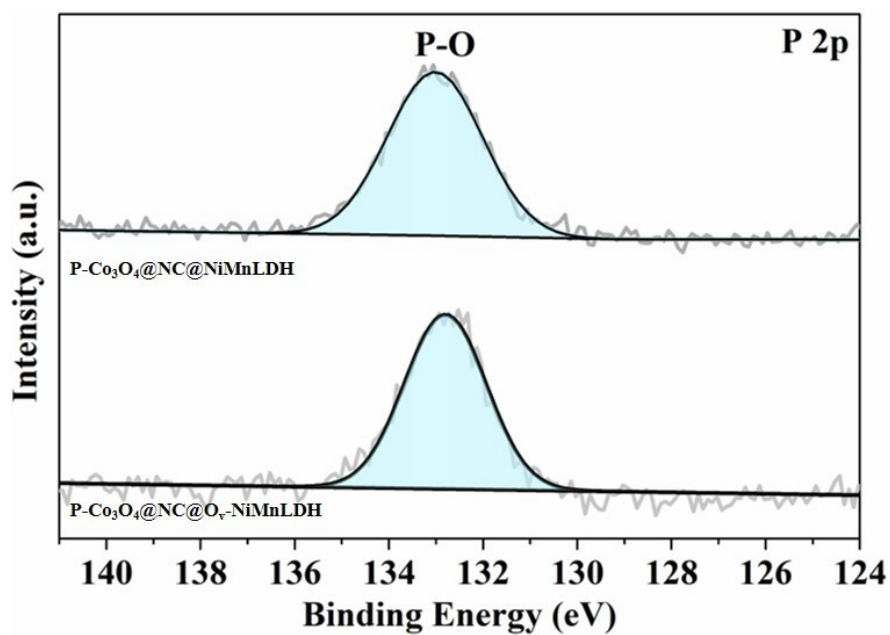


Fig. S5 P 2p XPS spectra of the P-Co₃O₄@NC@NiMnLDH and the P-Co₃O₄@NC@O_v-NiMnLDH electrode.

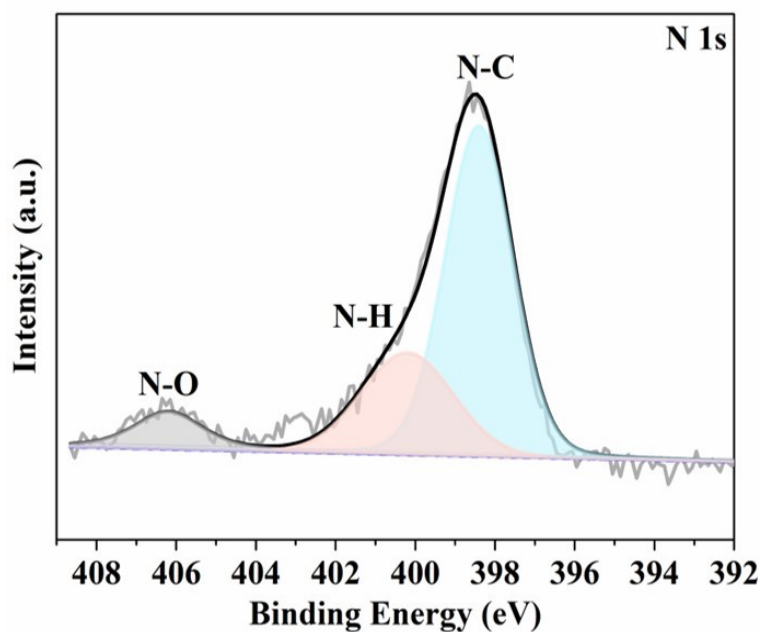


Fig. S6 N 1s XPS spectra of the P-Co₃O₄@NC@O_v-NiMnLDH.

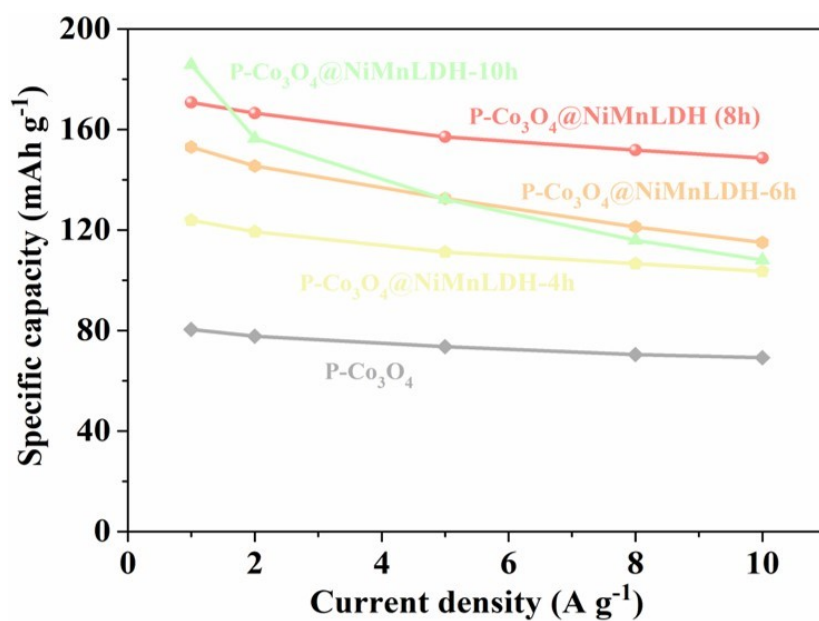


Fig. S7 The comparison of specific capacity of the as-prepared P-Co₃O₄@NC@NiMnLDH electrode with different LDH reaction time.

It can be seen from the figure that when the growth time of LDH is 8h, the electrode has the highest electrochemical charge discharge performance

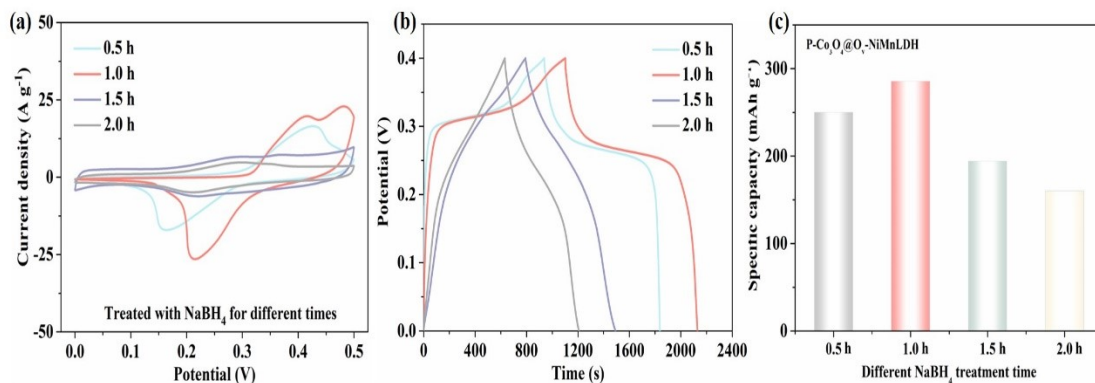


Fig. S8 The comparison of (a) CV curves at $5 mV s^{-1}$, (b) GCD curves at $1A g^{-1}$, (c) Specific capacity based on discharge time of the as-prepared $P-Co_3O_4@NC@O_v-NiMnLDH$ electrode with different $NaBH_4$ treatment times (0.5 h, 1 h, 1.5 h and 2 h).

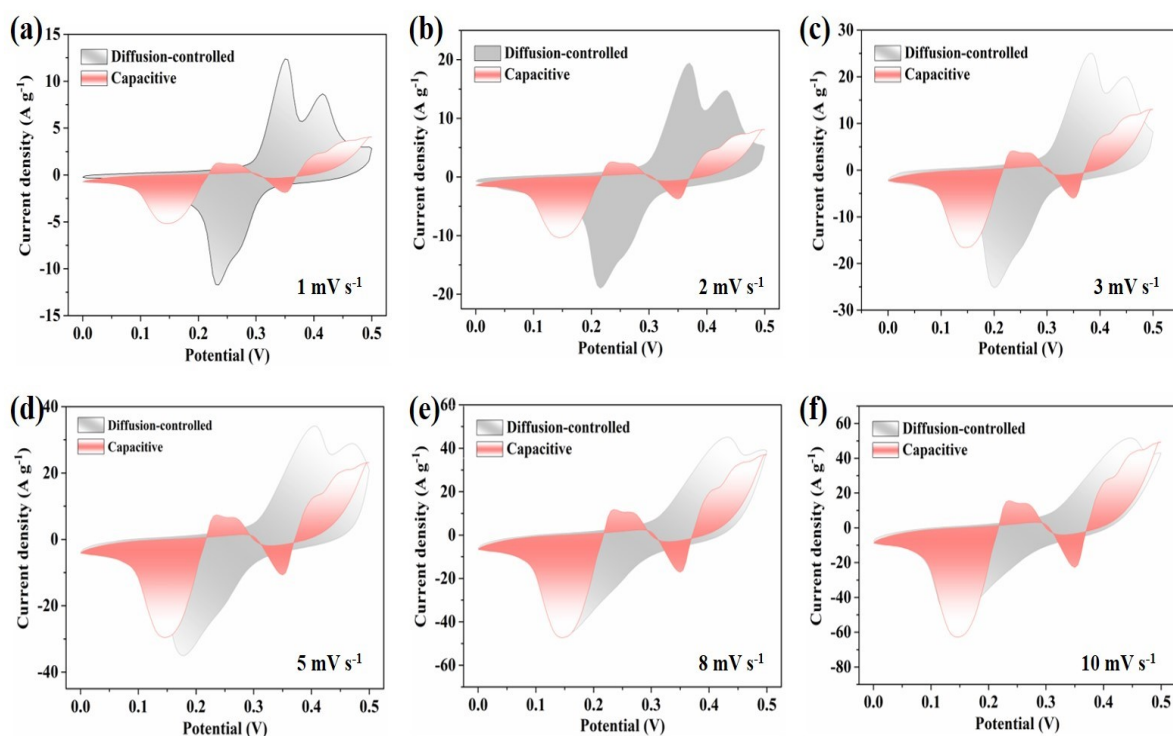


Fig. S9 The capacity analysis of the $P-Co_3O_4@NC@O_v-NiMnLDH$ electrode at different scanning rates.

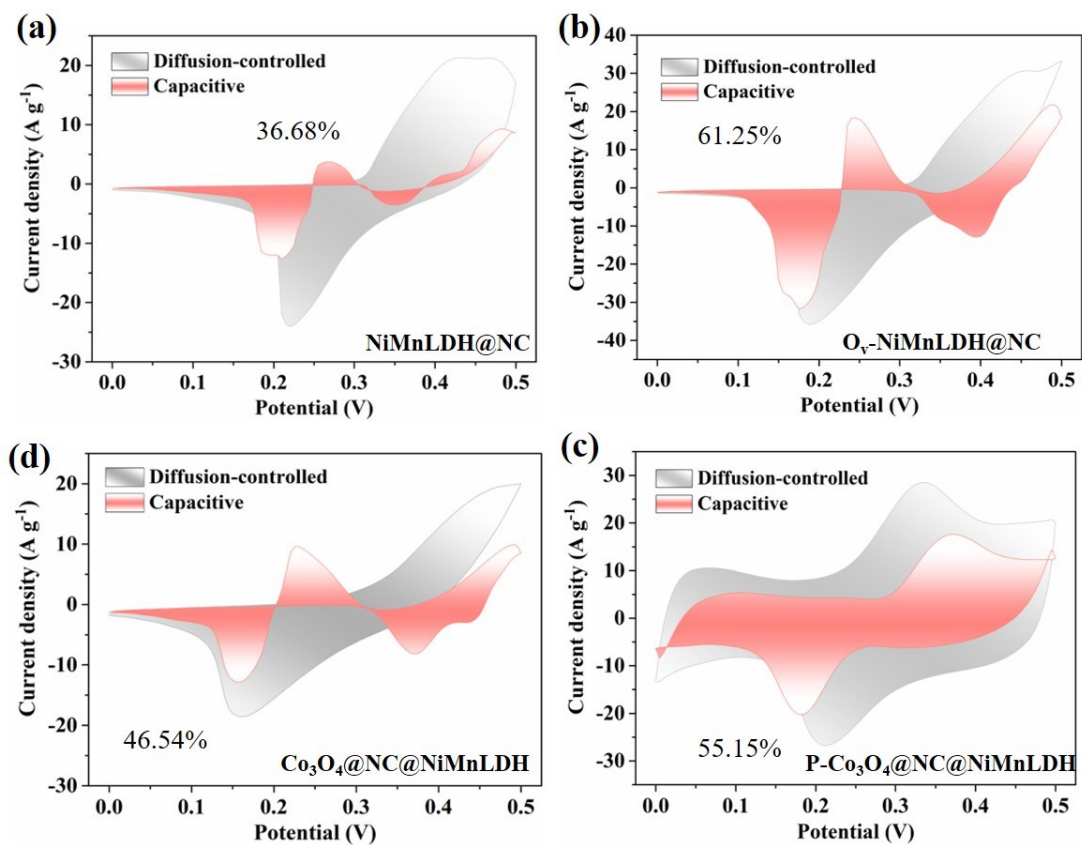


Fig. S10 The capacity analysis of the NiMnLDH@NC, O_v-NiMnLDH@NC, Co₃O₄@NC@NiMnLDH, P-Co₃O₄@NC@NiMnLDH electrode at 10 mV s⁻¹.

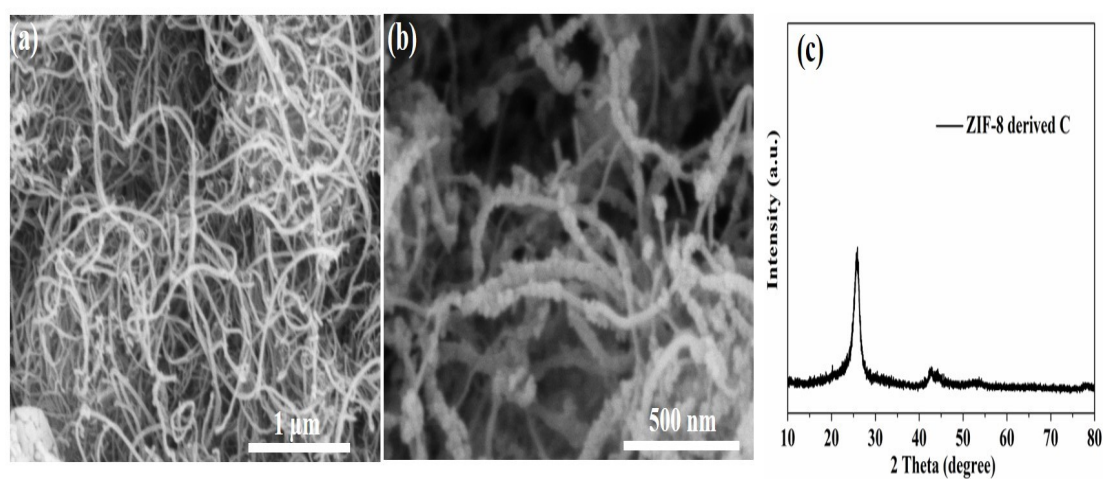


Fig. S11 The SEM image of (a) pure CNTs, (b) CNTs@ZIF-8 of derived carbon, (c) XRD of the CNTs@ZIF-8 of derived carbon.

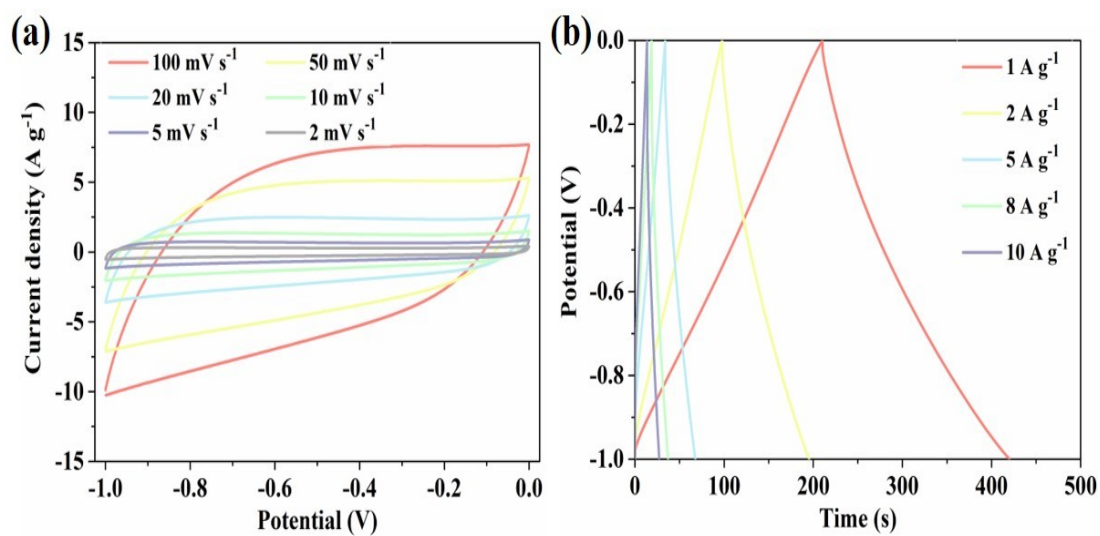


Fig. S12 (a) CV diagram of the prepared CNT@ZIF-8 derived carbon negative electrode, (b) GCD diagram of negative electrode.

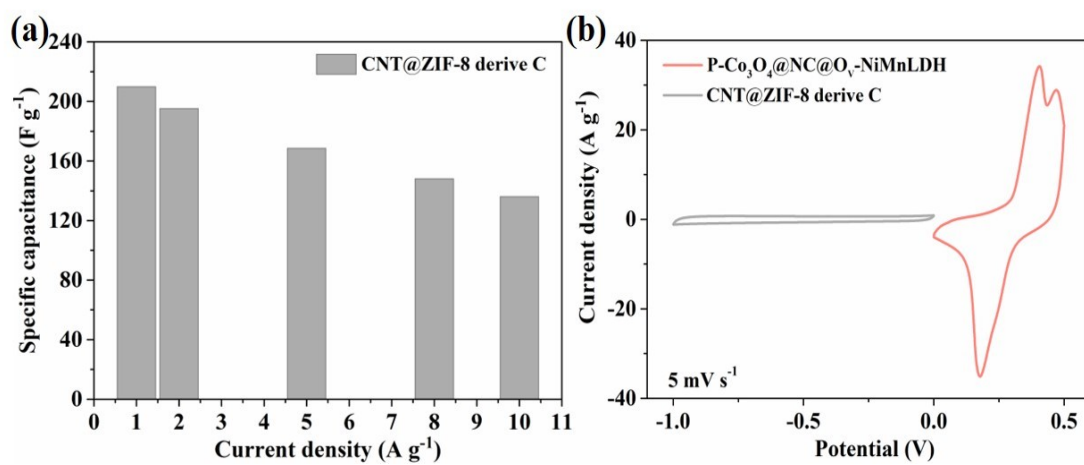


Fig. S13 (c) Mass specific capacitance diagram of negative electrode, (d) P-Co₃O₄@NC@O_v-NiMnLDH and CNTs@ZIF-8 derived C at scanning rate of 5 mV s⁻¹.

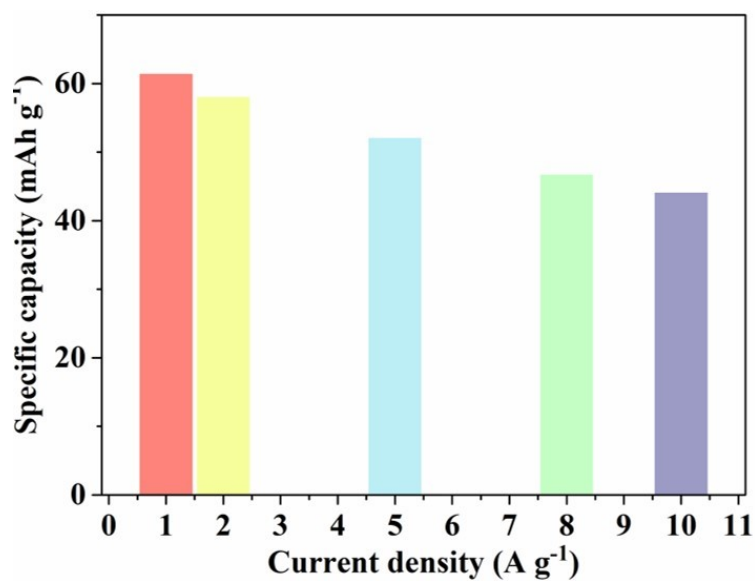


Fig. S14 The specific capacity of P-Co₃O₄@NC@O_v-NiMnLDH//CNTs@ZIF-8 derived C at different current densities.

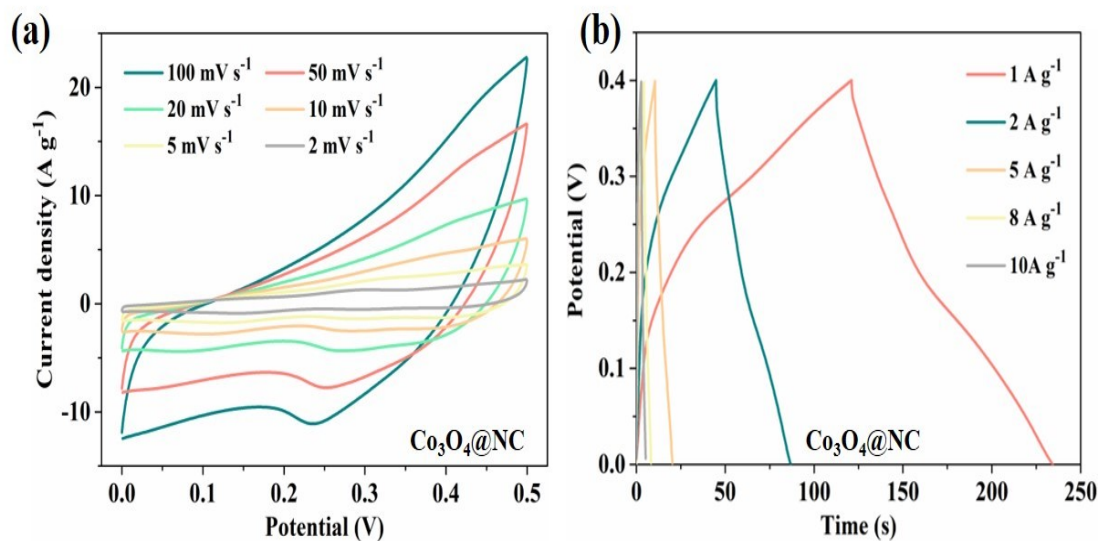


Fig. S15 (a) CV curves of Co₃O₄@NC at different scan rates, (b) GCD curves of Co₃O₄@NC at different current density.

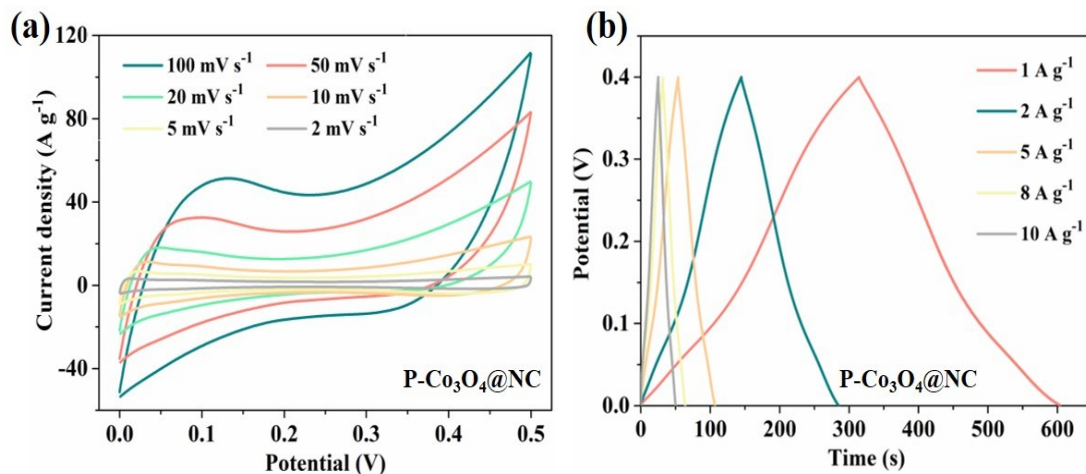


Fig. S16 (a) CV curves of P-Co₃O₄@NC at different scan rates, (b) GCD curves of P-Co₃O₄@NC at different current density.

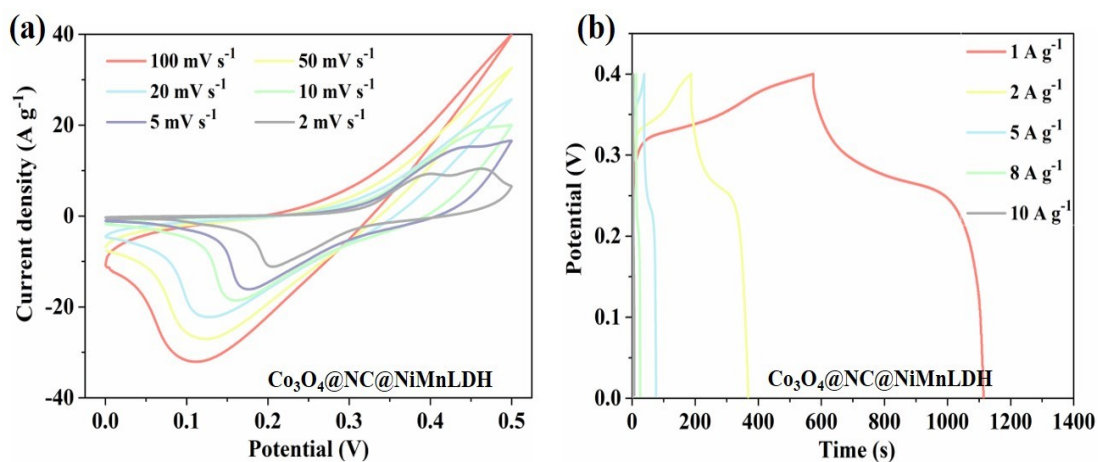


Fig. S17 (a) CV curves of Co₃O₄@NC@NiMnLDH at different scan rates, (b) GCD curves of Co₃O₄@NC@NiMnLDH at different current density.

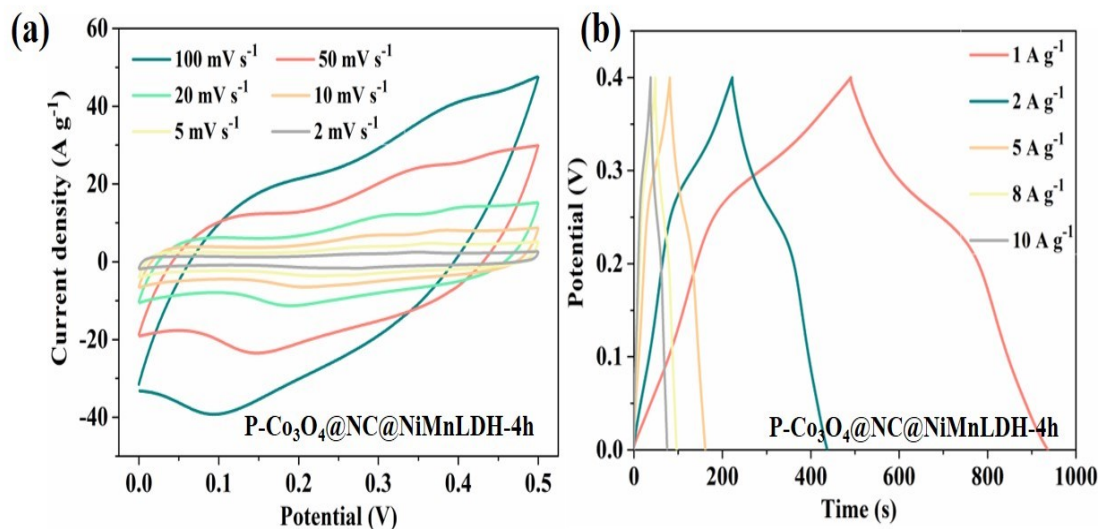


Fig. S18 (a) CV curves of $\text{Co}_3\text{O}_4@\text{NC}@\text{NiMnLDH-4h}$ at different scan rates, (b) GCD curves of $\text{Co}_3\text{O}_4@\text{NC}@\text{NiMnLDH-4h}$ at different current density.

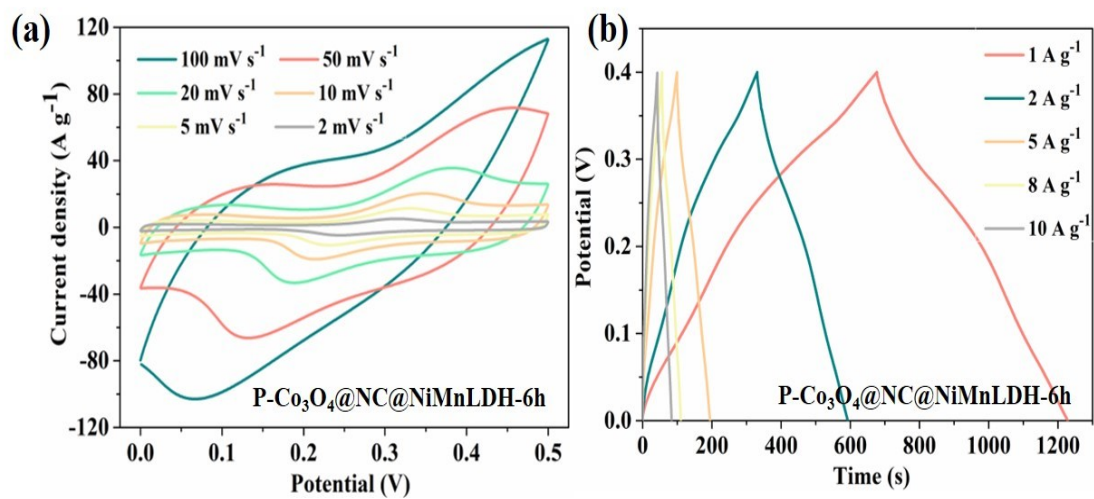


Fig. S19 (a) CV curves of $\text{Co}_3\text{O}_4@\text{NC}@\text{NiMnLDH-6h}$ at different scan rates, (b) GCD curves of $\text{Co}_3\text{O}_4@\text{NC}@\text{NiMnLDH-6h}$ at different current density.

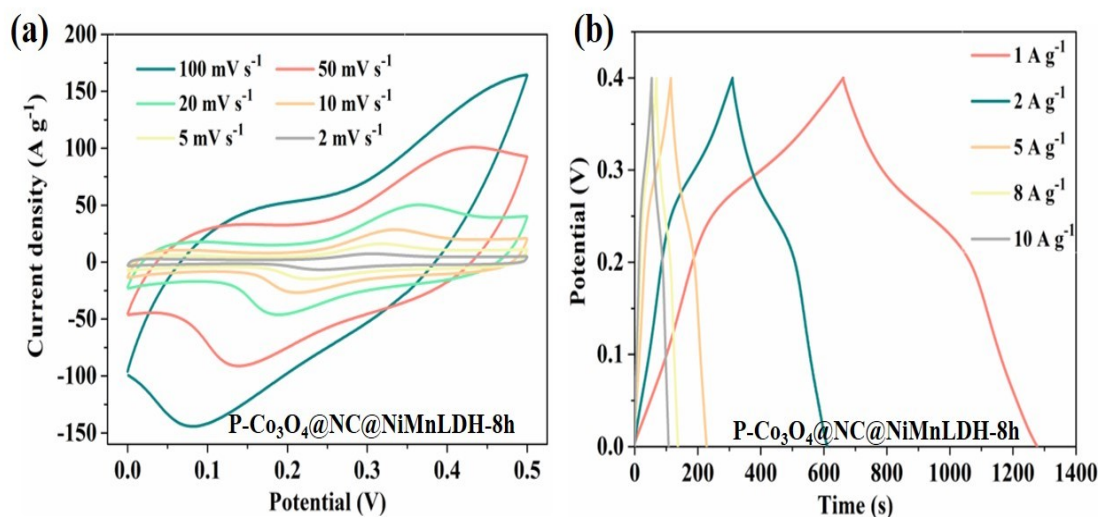


Fig. S20 (a) CV curves of $\text{Co}_3\text{O}_4@\text{NC}@\text{NiMnLDH-8h}$ at different scan rates, (b) GCD curves of $\text{Co}_3\text{O}_4@\text{NC}@\text{NiMnLDH-8h}$ at different current density.

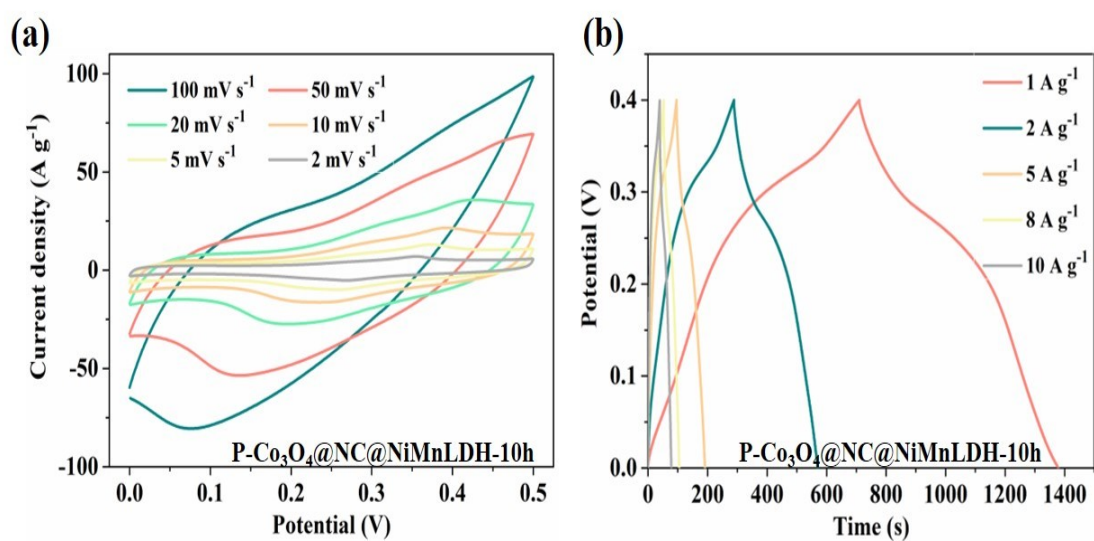


Fig. S21 (a) CV curves of $\text{Co}_3\text{O}_4@\text{NC}@\text{NiMnLDH-10h}$ at different scan rates, (b) GCD curves of $\text{Co}_3\text{O}_4@\text{NC}@\text{NiMnLDH-10h}$ at different current density.

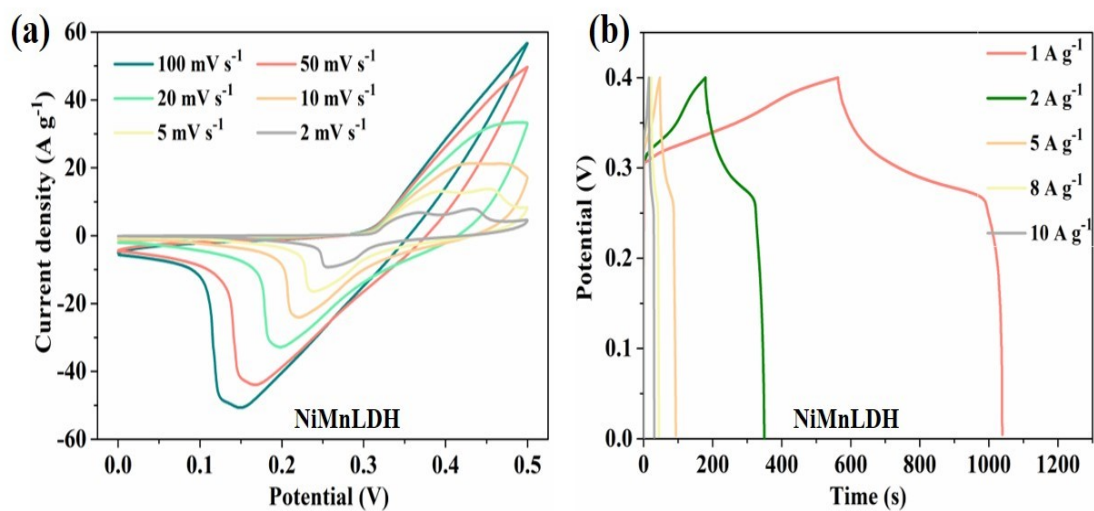


Fig. S22 (a) CV curves of NiMnLDH (8h) at different scan rates, (b) GCD curves of NiMnLDH at different current density.

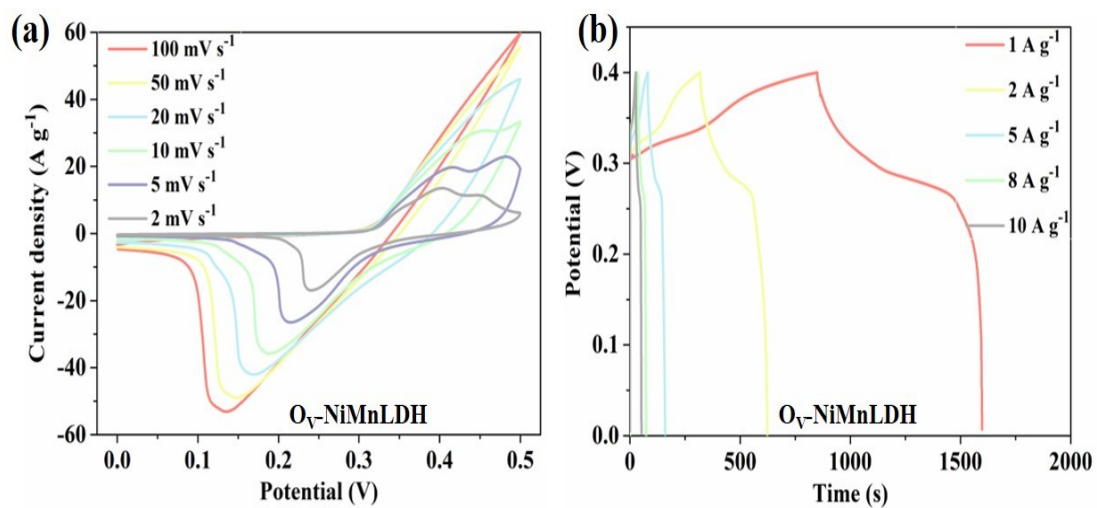


Fig. S23 (a) CV curves of O_v-NiMnLDH at different scan rates, (b) GCD curves of O_v-NiMnLDH at different current density.

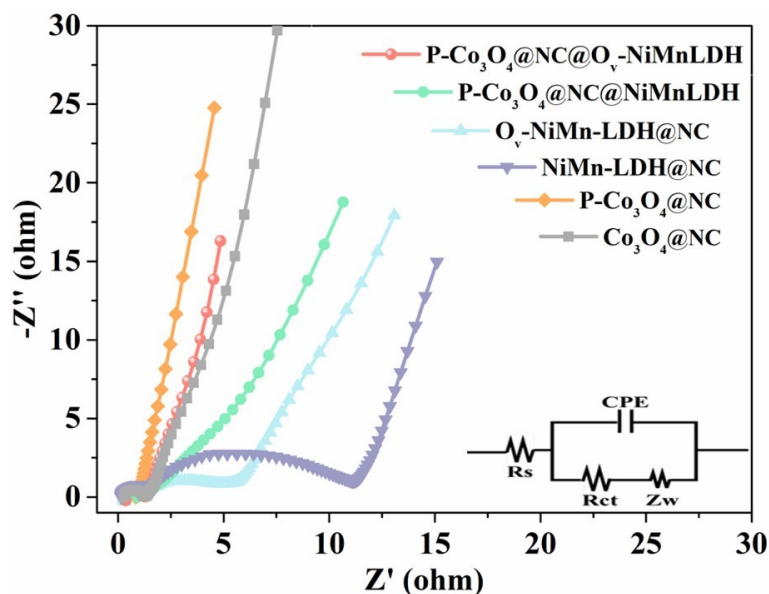


Fig. S24 EIS curves of as-prepared P-Co₃O₄@NC@O_v-NiMnLDH electrode and all comparison electrode samples and the built-in diagram is the equivalent circuit diagram.

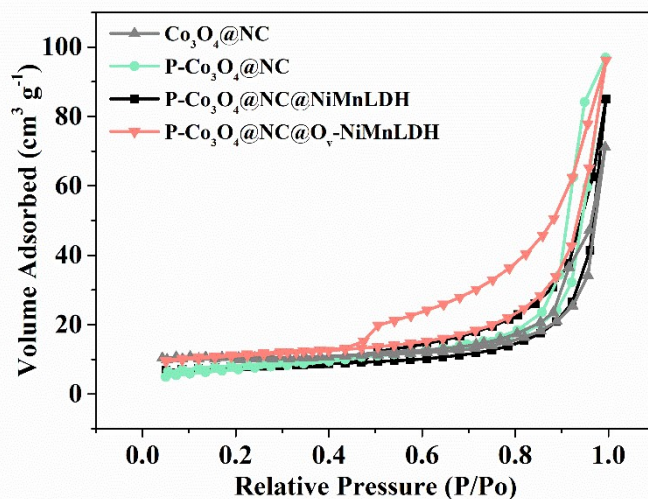


Fig. S25 The comparison of the BET data of the as-synthesized P-Co₃O₄@NC@O_v-NiMnLDH, the Co₃O₄@NC, the P-Co₃O₄@NC and the P-Co₃O₄@NC@NiMnLDH electrode.

The samples used in the BET test were scraped from carbon fibers. The BET surface area of the as-synthesized Co₃O₄@NC, P-Co₃O₄@NC, P-Co₃O₄@NC@NiMnLDH and P-Co₃O₄@NC@O_v-NiMnLDH sample is 28.96 m² g⁻¹, 35.30 m² g⁻¹, 24.66 m² g⁻¹ and 27.81 m² g⁻¹, respectively. Compared with the

$\text{Co}_3\text{O}_4@\text{NC}$ electrode, the BET area of $\text{P-Co}_3\text{O}_4@\text{NC}$ was slightly increased due to P-doping. The subsequent growth of NiMnLDH covered the $\text{Co}_3\text{O}_4@\text{NC}$ electrode surface, resulting in a slight decrease in the BET area of $\text{P-Co}_3\text{O}_4@\text{NC}@\text{NiMnLDH}$. Then, compare with the $\text{P-Co}_3\text{O}_4@\text{NC}@\text{NiMnLDH}$ electrode, the further introduction of oxygen vacancies makes the BET area of $\text{P-Co}_3\text{O}_4@\text{NC}@\text{O}_v\text{-NiMnLDH}$ electrode slightly increased. However, on the whole, the BET values are almost close, indicating that the synthesized P-doping site and oxygen vacancy active site play a major role.

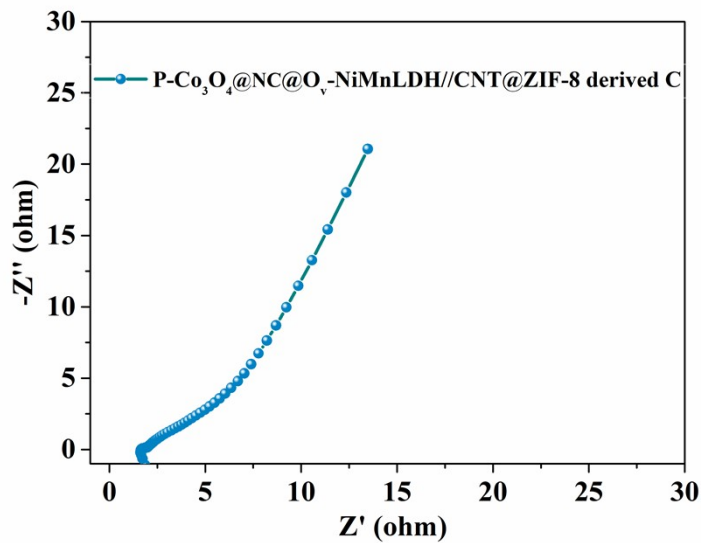


Fig. S26 The EIS data of the as-prepared $\text{P-Co}_3\text{O}_4@\text{NC}@\text{O}_v\text{-NiMnLDH//CNT@ZIF-8}$ derived C ASC device.